# Operation of the 56 MHz superconducting rf cavity in RHIC with higher order mode damper

Qiong Wu,[1,*] Sergey Belomestnykh,[2,3] Ilan Ben-Zvi,[1,3] Michael M. Blaskiewicz,[1] Thomas Hayes,[1] Kevin Mernick,[1] Freddy Severino,[1] Kevin Smith,[1] and Alex Zaltsman[1]

[1]*Brookhaven National Laboratory, Upton, New York 11973, USA*
[2]*Fermilab, Batavia, Illinois 60510, USA*
[3]*Stony Brook University, Stony Brook, New York 11790, USA*

(Received 11 April 2019; published 29 October 2019)

A 56 MHz superconducting rf cavity was designed and installed in the Relativistic Heavy Ion Collider (RHIC). It is the first superconducting quarter wave resonator (QWR) operating in a high-energy storage ring. We discuss herein a design of the cavity and its key components and the cavity operation with Au + Au collisions, and with asymmetrical Au + $^3$He collisions. The cavity is a storage cavity, meaning that it becomes active only at the energy of the experiment, after the acceleration cycle is completed. Without beam, the cavity reached 1.93 MV and a $Q_0$ of $3.0 \times 10^8$ after helium conditioning. The cavity voltage was limited at 300 kV with beam operation due to heating in the Higher Order Mode (HOM) coupler. With the cavity operating at 300 kV, an improvement in luminosity was detected from direct measurements, and the bunch length has been reduced. The uniqueness of the QWR necessitated development of an innovative design of the higher order mode dampers with high-pass filters, and a distinctive fundamental mode damper that enables the cavity to be transparent to the beam during acceleration.

DOI: 10.1103/PhysRevAccelBeams.22.102001

## I. INTRODUCTION

RHIC was designed with accelerating and storage rf systems to operate at harmonic numbers $h = 360$, and $h = 7 \times 360 = 2520$, which correspond to frequencies of 28.15 MHz and 197.05 MHz, respectively [1]. The five 197 MHz copper cavities installed in each ring are used to store bunches for up to 10 hours after they have been accelerated to the top energy. With the current RHIC operational settings, the typical full length of the 100 GeV Au beam is 9.7 ns with the 28 MHz acceleration rf system. The bucket length of the relatively high frequency storage cavities is 5.1 ns, which is not sufficient to accommodate the ion bunches without going through the rf gymnastics of bunch rotation, or rebucketing. However, this rebucketing process causes an increase in longitudinal emittance due to nonlinearity and hardware complications. The longitudinal emittance increase leads to 30% of the particles being spilled into neighboring buckets, which hardly contribute to the luminosity at collision.

A storage cavity at a frequency of 56.3 MHz was proposed in 2007 to provide adequate rf acceptance to long bunches without rebucketing [2]. With 2 MV operation voltage, the longitudinal acceptance using the 56 MHz cavity at RHIC is 6.4 eV s/u for 100 GeV/u gold ions and 15.5 eV s/u for 250 GeV protons, in both cases much larger than the beam emittance [3]. At the same longitudinal emittance, the full bunch length with the 56 MHz rf system may be suppressed to below the bucket size of the 197 MHz cavity. As it was shown from direct luminosity measurements during RHIC operation in 2014, the combination of the 56 MHz and 197 MHz rf systems raised the luminosity within the vertex of the detectors, which will be discussed in the later section of this paper. The 56 MHz rf cavity installed in RHIC is the first quarter wave superconducting resonator for storage rings, which is designed to provide a high gap voltage to above 2 MV at the low frequency of 56 MHz. With such an advantage, the number of cavities at RHIC can be reduced to just one, which is further shared by both rings, and therefore has somewhat lowered the RHIC impedance. The cavity operates with the beam traversing through its axis. This design provides a compact size making feasible its installation in the existing tunnel. The 56 MHz cavity is beam driven, although a maximum of 4 kW rf power is provided from an amplifier for controlling its amplitude and for overcoming the detuning due to microphonic. After the beam has been accelerated to

*qiowu@bnl.gov

top energy, the cavity is tuned toward the beam frequency from below. Since the cavity operates above the transition energy, Robinson instability is avoided [4,5]. Nevertheless, external rf power is necessary to ensure stability of its amplitude against ponderomotive instabilities [6,7]. The instability of the coupled bunch of the ring-cavity system was studied [8], and damping is provided accordingly to the higher order modes to the specified thresholds for passing through the transition energy and at store.

## II. 56 MHz CAVITY AND ITS KEY COMPONENTS

### A. Cavity

The 56 MHz SRF cavity is a quarter-wave resonator with beam passing along its axis of symmetry, as shown in Fig. 1. The cavity is located in the common section of the RHIC, and shared by ion bunches from both rings. Serving both rings with one cavity provides cost benefits for construction and operation [9]. To achieve identical longitudinal dynamic effects for both beams, the difference in rf phase must be equal to $\pi$. The two colliding beams are synchronized at the interaction point (IP). Thus the cavity should be installed such that the accelerating gap is located at $(n + 1/4)\lambda$ away from the IP. The wavelength at a frequency of 56.3 MHz is $\lambda = 5.33$ m. The available position in RHIC is located at $1.25\lambda$, which is 6.66 m from the IP. The parameters of the cavity operating at 2 MV are shown in Table I.

The cavity is basically a standard quarter wave resonator. Considering the height limit inside the RHIC tunnel to accommodate the full cryomodule and sufficient headroom for its cryogenic system, the cavity diameter was set to less than or equal 50 cm. By optimizing the shape locally near the acceleration gap, the cavity design aimed at both decreasing the ratio of the peak electric field to the accelerating field and increasing the sensitivity of the tuning plate [10].

#### *1. Tuning*

The cavity is tuned by pushing and pulling the beam pipe which then acts on a flat tuning plate at the accelerating gap, as shown in Fig. 1. To change the frequency, the flat tuning plate of the cavity is connected to the cylindrical body with a 1 mm thin Nb membrane, as shown in Fig. 2. This mechanically vulnerable thin connecting section is separated from other environments by a torispherical dome, so that the tuning plate is not exposed to any differential pressure. Before the final chemical treatment, a pretuning procedure was performed by plastically deforming the tuning plate connecting section. The pretuning pulled the tuning plate with the cylindrical cavity body fixed and increased the length of the cavity by 2.8 mm, which corresponds to a frequency increase of 72.5 kHz. During the operation phase, the entire elastic tuning range is 46.25 kHz, which corresponds to a 3 mm movement of the beam pipe. During operation, the cavity is tuned 34 kHz below the beam revolution frequency in order to minimize the beam-excited cavity voltage to a negligible level. A piezo-electric tuner provides fine frequency tuning and a fast response in addition to the slower but larger range

TABLE I. Cavity parameters.

| Parameter | Unit | Value |
|---|---|---|
| Frequency | MHz | 56.30 |
| Length | cm | 134.88 |
| Gap | cm | 8.45 |
| Outer diameter | cm | 50.5 |
| Aperture | cm | 10.0 |
| Operating temp | K | 4.5 |
| $R/Q$ | Ω | 80.5 |
| $Q_0$ | | $1.95 \times 10^9$ |
| G | Ω | 21.84 |
| $E_{acc}$ | MV/m | 23.50 |
| $E_{peak}/E_{acc}$ | | 1.77 |
| $B_{peak}/E_{acc}$ | mT/MV/m | 3.81 |

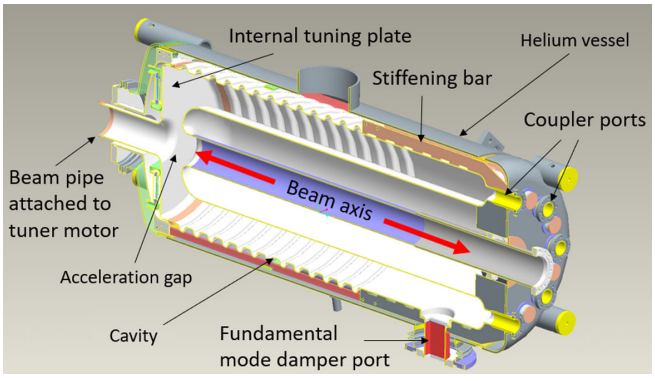


FIG. 1. 56 MHz SRF cavity with a total length of 1.3 meters.

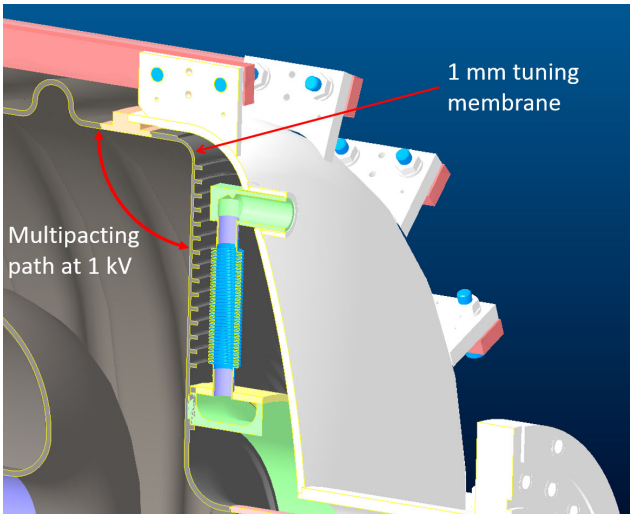


FIG. 2. Tuning section of 56 MHz cavity with push-pull on 1 mm Nb membrane for changing the cavity volume.

stepper motor tuner, and potentially can compensate detuning due to microphonic noise.

#### *2. Multipacting*

As the cavity has a traditional coaxial shape, multipacting is easily excited, primarily in the space between the parallel walls of inner and outer conductors, including single-point multipacting originating on the outer conductor. For suppressing this multipacting, thirteen corrugations were implemented on the outer wall [11]. The secondary electrons, when entering the corrugation region, their path lengths will deviate from their resonance condition. Therefore, there is no local accumulation of multipacting electrons. The corrugations are 2 cm in height, with 6 cm spacing. Simulations showed that only the first 70 cm from the cavity gap has an electric field strong enough for the resonance condition.

However, during cavity testing prior to operation with beam, multipacting barriers were encountered at low gap voltages. The first barrier, at 1 kV cavity gap voltage, is a two-point multipacting across the corner of the tuning membrane as shown in Fig. 2, conditioned away with 1 kW RF power and external $Q$ of the fundamental mode coupler of $10^6$. The strongest multipacting region covers a gap voltage range from 90 kV to 140 kV. These multipacting barriers were not predicted in previous simulation works [12], and need further analysis. With the 1 kW amplifier running in the CW mode, the multipacting zone was conditioned away after 30 minutes. The cavity required multipacting conditioning after its installation in the RHIC beam line for several hours incrementally. After all the conditionings, the cavity voltage ramped smoothly during its continuous operation with full intensity RHIC beam over a period of 18 days.

### B. Couplers

The cavity does not have sufficient tuning range to follow the large change in frequency during the RHIC energy ramp, so it is tuned up to the resonance frequency only after reaching the store energy. To make the cavity's fundamental mode transparent to the beam current during the beam energy ramp, a fundamental mode damper (FMD) is inserted into the cavity from a rectangular port opened on the side. The fully inserted FMD is shown in Fig. 3. The FMD is located with its center axis at 114.3 cm from the tuning plate. The strong coupling of this coupler detunes the cavity frequency during its insertion and extraction processes, therefore the FMD has a carefully chosen location to have a minimum frequency shift by balancing the capacitive and inductive effects. The loaded $Q$ and the frequency change due to the motion of the FMD is shown in Fig. 3. A combination of the tuning plate and fully inserted FMD detunes the cavity frequency by 68.5 kHz from the beam resonance. When FMD is fully inserted, the cavity loaded $Q$ value is 309. The cavity voltage, excited by

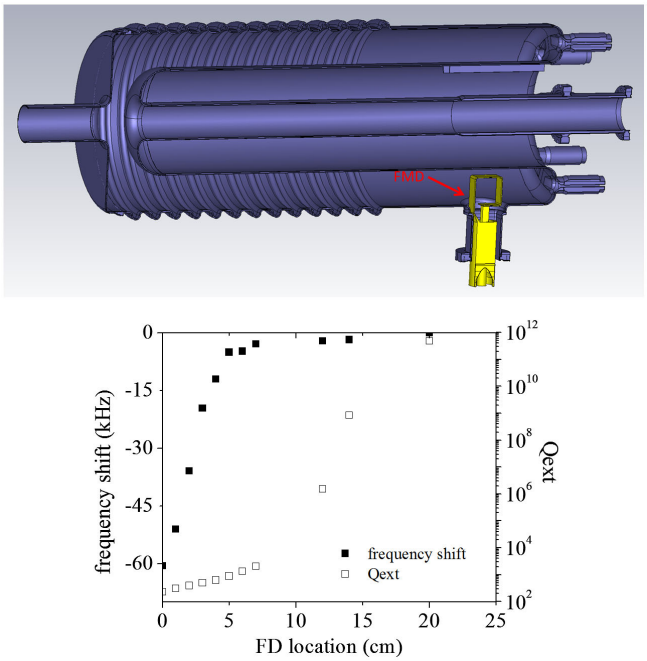


FIG. 3. Top: The fundamental mode damper fully inserted into the cavity. Bottom: The cavity loaded $Q$ and frequency change versus FMD location. Zero FD location corresponds to fully inserted.

the full intensity RHIC beam after the large detuning and heavy damping, is less than 6 kV.

The 56 MHz cavity is operated as a beam driven resonator, whose energy is built up by beam loading and supplied from the 28 MHz main accelerating system. In addition, an external amplifier with a maximum power of 4 kW is connected to the cavity via a fundamental power coupler (FPC). The loop-shaped FPC, located in the maximum magnetic field region, is shown in Fig. 4. Insertion of the FPC is variable via a stepper motor, and the external $Q$ changes over two orders of magnitude. Due

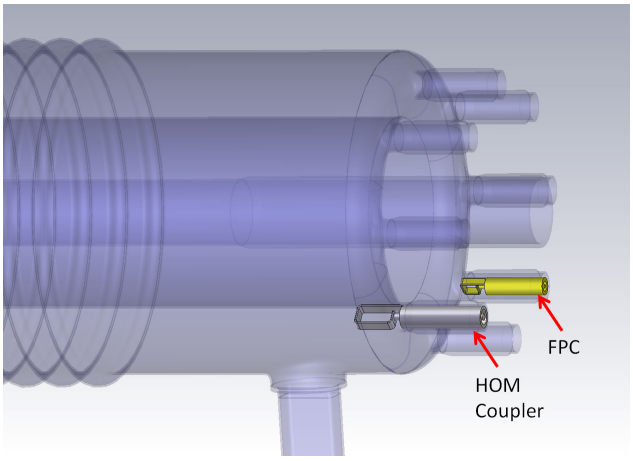


FIG. 4. FPC (yellow) and HOM coupler (grey) locations in the cavity.

to small losses of the superconducting cavity, the amplifier power alone is sufficient for driving the cavity to above 2 MV on resonance and initial conditioning. During conditioning, the FPC is parked in its fully inserted position with an external $Q$ of $2.2 \times 10^6$ to maximize the transmitted rf power to the cavity. During operation, the FPC couples rf power into the cavity to compensate the amplitude change in the gap voltage, which then is used as the real time correction of the voltage. The optimum coupling of the FPC is $\beta = 79$, which corresponds to an external $Q$ of $2.2 \times 10^7$ [13].

The higher order modes (HOMs) of the cavity are damped through an HOM loop-shaped coupler, as shown in Fig. 4. The insertion of FMD breaks the cavity field in axial symmetry, therefore the orientation of the multipole modes are perturbed by its insertion and the location of the HOM coupler is specifically chosen for attaining a balanced optimum damping of HOMs. For all HOMs below 700 MHz, we measured that the coupler damps power of all dipole modes by 5 orders of magnitude and of quadrupole modes by 6 orders of magnitude. The HOM coupler loop couples to all modes, including the fundamental mode. To avoid dangerously large amount of power from the fundamental mode being sent into the HOM coupler load, a Chebyshev high-pass filter was connected to the coupler loop. The frequency of the first HOM is 168 MHz. Thus, the frequency difference between the fundamental mode and the first HOM is greater than 100 MHz, which simplifies the filter design. The HOM coupler and filter are discussed in the next section in detail.

### C. HOM couplers with high pass filter

For the HOM analysis of the 56 MHz SRF cavity, we define the $R/Q$'s as the following:

$$\frac{R}{Q}_{\text{monopole}} = \frac{V^2}{\omega U} = \frac{|\int E_{z,\text{axis}} \exp(ikz) dz|^2}{\omega U}$$

$$\frac{R}{Q}_{\text{dipole}} = \frac{1}{k^2 d^2}\frac{V^2}{\omega U} = \frac{1}{k^2 d^2}\frac{|\int E_{z,d} \exp(ikz) dz|^2}{\omega U}$$

$$\frac{R}{Q}_{\text{quadrupole, sextupole}} = \frac{V^2}{\omega U} = \frac{|\int E_{z,d} \exp(ikz) dz|^2}{\omega U}$$

where $\omega$ and $U$ are the frequency and stored energy of the specified mode, $k = \omega/c$ is the wave number, $z$ is the direction along the cavity symmetry axis, $E_{z,\text{axis}}$ and $E_{z,d}$ are the electric fields in the $z$ direction on the axis and with a offset of $d$. The $R/Q$'s of the monopole and dipole modes are, as plotted in Fig. 5, distributed between 0 to 100, while the $R/Q$'s of the quadrupoles and sextupoles are all below $10^{-2}$. Therefore, while the effective damping for all the modes is important, the monopole and dipole modes are more critical with respect to the other two types.

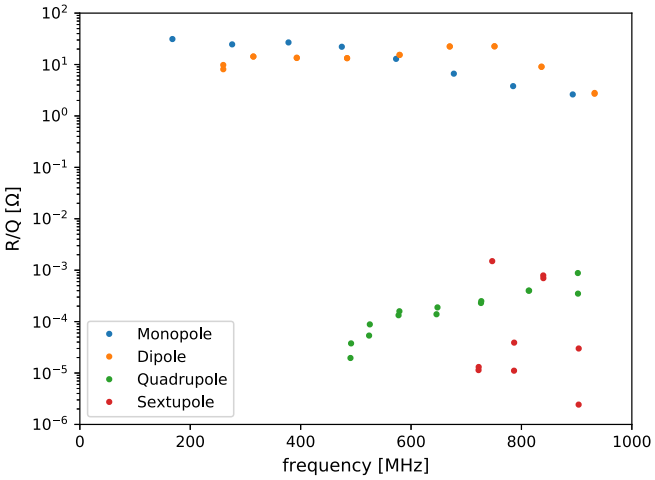


FIG. 5. $R/Q$ of all cavity modes.

#### 1. HOM coupler loop

We chose the chemical cleaning ports as the insertion ports for the HOM couplers to prevent extra penetrations on the cavity. All the chemical cleaning ports are located in the peak magnetic field region of the cavity, thus the HOM coupler design adopted a rectangular loop with an opening area of 6 cm × 2.88 cm, see Fig. 6. The width of the loop was set as 2 cm and its thickness at 0.3 cm. The size of the coupler loop was designed to provide sufficient inductive coupling, while also allowing enough clearance through the 4 cm diameter opening of the port. The width of the loop is chosen to contain enough material for thermal conduction. To limit the peak surface field of the HOM coupler to below 80 mT during operation, the thickness of the loop is set to be below 0.5 cm.

Since the size of the damper loop is limited by the port opening, the initial design of the cavity was with multiple HOM dampers installed. Out of 8 ports, 4 are occupied by the fundamental power coupler, pick-up probe, and two IR sensors for multipacting detection. Thus, we are limited to 4 HOM dampers to fulfill the damping requirement of the 56 MHz SRF cavity. All 8 chemical ports are distributed

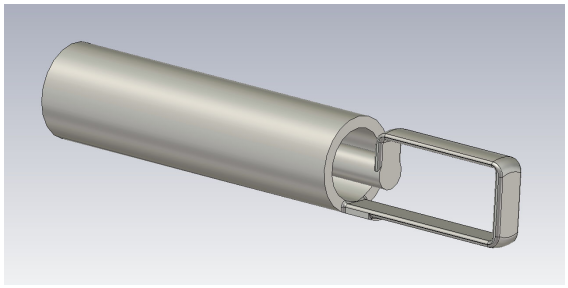

FIG. 6. HOM coupler loop.

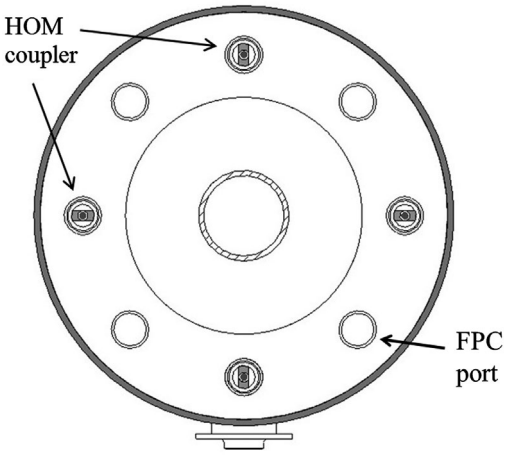


FIG. 7. End view of the cavity with symmetrical distribution of the HOM couplers.

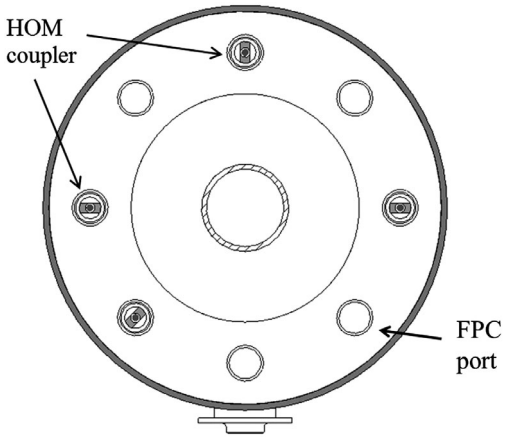


FIG. 9. End view of cavity with asymmetrical distribution of the HOM couplers.

uniformly around the cavity end. The choice of the ports selected for HOM coupler insertion is determined by the damping effect [14]. As shown in Fig. 7, initially the couplers were inserted 90 degrees apart from each other in a symmetrical pattern. All the loops are oriented radially as shown in the figure to maximize the effective coupling area.

The FMD port breaks the cavity axial symmetry, therefore the orientation of the multipole modes are determined accordingly. As for the dipole modes, the configurations are either aligned with or perpendicular to the FMD port. As shown by the orange dots in Fig. 8, the 4 HOM couplers can effectively damp all the dipole modes. The green dots representing the quadrupole modes in Fig. 8 are separated into two sets: with the external $Q$ ($Q_{\mathrm{ext}}$) value of below $10^5$ and above $10^8$. The low $Q_{\mathrm{ext}}$ values are associated with the quadrupole modes that are oriented in the same configuration as of the couplers, while high $Q_{\mathrm{ext}}$ values are for the orthogonal modes. High $Q_{\mathrm{ext}}$ indicates the damping of the corresponding modes is not sufficient.

To provide coupling to orthogonal quadrupole HOMs, the four dampers must be placed asymmetrically, as shown in Fig. 9. In this scheme, the bottom HOM coupler is rotated clockwise by 45 degrees, so that it will have strong coupling with the quadrupole modes missed by the other three couplers. Figure 10 shows that all the $Q_{\mathrm{ext}}$ in such an asymmetrical configuration of the HOM couplers are under $10^5$. As a result of the HOM coupler position change, the coupling to the vertical dipole modes is decreased, but the difference is small. Sufficient damping is provided to all the modes, while damping to the monopole and dipole modes is more than an order of magnitude stronger than the other two types of modes.

HOM coupling is analyzed with MicroWave Studio (MWS) 3D simulation software [15].

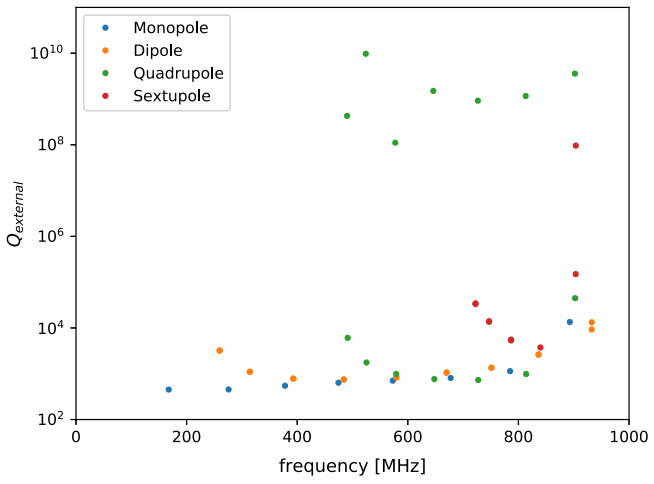


FIG. 8. HOM coupling from symmetrically distributed couplers.

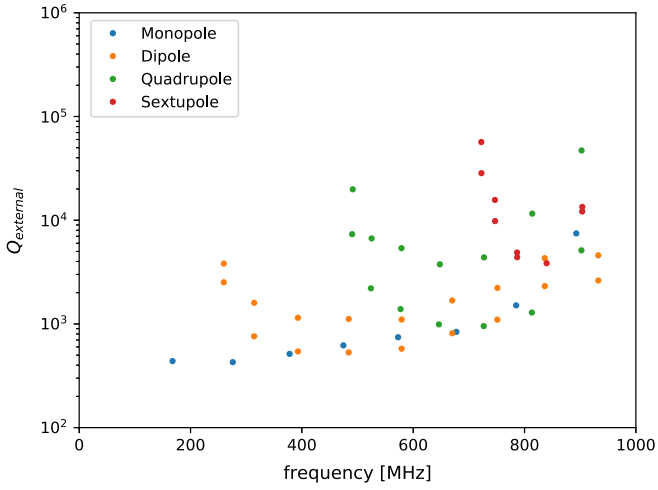


FIG. 10. HOM coupling from asymmetrically distributed couplers.

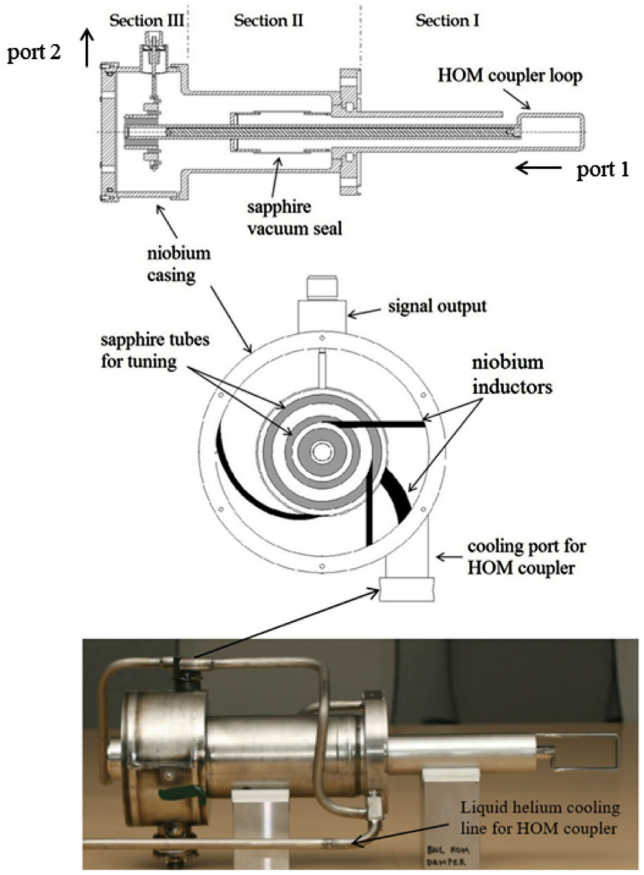


FIG. 11. Top: Cross section view of the HOM coupler with high-pass filter assembly, with port 1 and port 2 labeled for filter measurements. Middle: End view of the high pass filter. Bottom: HOM Coupler with high-pass filter and cooling channels fabricated at Jefferson Lab.

### *2. High-pass filter*

The HOM dampers will remain in the cavity during operation. Therefore, all modes, including the fundamental mode, will be coupled out. According to our MWS simulation, the loaded $Q$ of the fundamental mode of the cavity will drop to about $10^3$. Compared to the designed loaded $Q$ of $4 \times 10^7$, this will send a dangerously large amount of power into the HOM damper load. The frequency of the first HOM is 168 MHz, and thus, the frequency difference between the fundamental mode and the first HOM is greater than 110 MHz. With such a large separation, we designed and incorporated a high-pass filter into the circuit to reject the fundamental mode while allowing all HOMs to propagate. In addition to reflecting the fundamental mode, the filter must contain a vacuum seal to separate the ultra-high vacuum in the cavity from the insulation vacuum. Because the cavity is superconducting, the design of the filter must be such to also prevent excessive heat transfer into the HOM coupler and thus raising the temperature in the vicinity of the cavity. Furthermore, since the ports for the HOM couplers are needed to allow access for chemically treating the cavity, the entire HOM coupler assembly must be detachable from the cavity.

We designed the filter as a three-stage high-pass Chebyshev T-Type filter to obtain a steep roll-off and minimize the error between the designed and the actual object, Fig. 11. In the cross-sectional view, the assembly has been separated into three sections with a total length of 44.6 cm. Section I is the HOM loop that penetrates completely into the cavity, along with the coaxial structure for lossless transport of the rf power. Section II is the seal for the cavity's ultrahigh vacuum. The center and outer conductors of the coaxial line are joined by a sapphire tube brazed onto two niobium cuffs, which then are welded to the two conductors. The sapphire tube is 6.35 cm long and can withhold more than 3 MV. Section III is the high pass filter structure. Three coaxial sapphire rings, shown in grey, with niobium spacers constitute the three capacitors in the design; the four inductors are niobium rods, shown in black, with carefully chosen lengths and locations. All the niobium rods start on one of the niobium cuffs, with their other end being welded on the outer can of the high pass filter. An end view in the middle of Fig. 11 shows all the sapphire rings and niobium rods for the filter. We selected sapphire due to its low loss tangent, to reduce heat dissipation in the HOM damper caused by dielectric heating. To ensure better conductive cooling of the loop, we designed the filter with an inductor first, as shown in the lumped circuit diagram and the assembly after fabrication in Fig. 12. The center conductor of the coaxial structure and the first inductor both are fabricated with niobium tubes, and high RRR copper rods are inserted into these tubes leaving a clearance for thermal expansion.

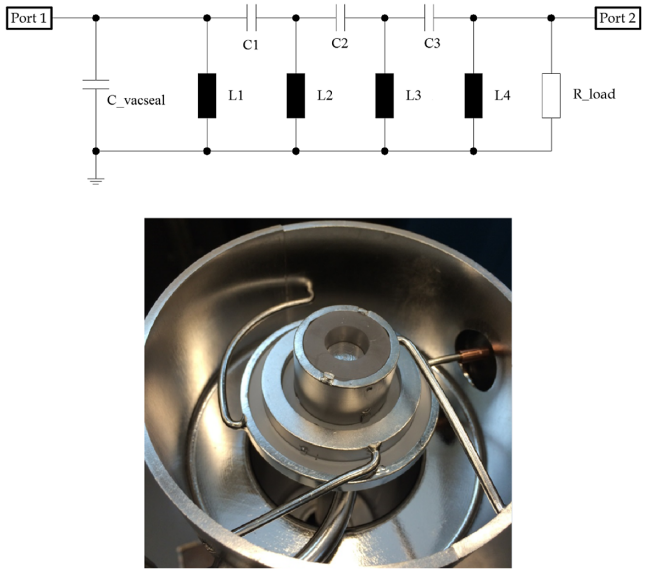


FIG. 12. Top: Simplified RLC circuit of the high-pass filter. Bottom: High-pass filter section in the HOM coupler.

TABLE II. Components of the equivalent circuit for the high pass filter.

| Component | Unit | Capacitance/Inductance |
|---|---|---|
| $C_{vacseal}$ | pF | 0.41 |
| $C_1$ | pF | 23.1 |
| $C_2$ | pF | 24.9 |
| $C_3$ | pF | 13.3 |
| $L_1$ | nH | 40.3 |
| $L_2$ | nH | 40.1 |
| $L_3$ | nH | 37.5 |
| $L_4$ | nH | 75.8 |

The copper rods are welded together at the joint to serve as a low-thermal-conductivity cooling path for heat generated at the HOM coupler loop. The niobium tube of the first inductor is welded onto the filter outer case, while the inner copper rod extends through the joint into a small vacuum sealed cooling port, as shown in Fig. 11. The cooling port has two transfer lines connected to the main liquid helium supply line on top of the cavity. During operation, the small chamber of the cooling port is filled with liquid helium through these lines with the end of the copper rod immersed into the 4 K liquid. rf heat generated at the coupler loop is transferred through the connected copper rods in both the center conductor and the first inductor in to the liquid helium bath in the cooling port.

We calculated values of the lumped RLC circuit individually according to the actual components in the design; Table II gives the results. Here, we also took into account the different dielectric constant for sapphire in its radial and azimuthal direction of the anisotropy axis at 4.2 K. Port 1 corresponds to the input of coaxial structure after the coupler loop, while port 2 corresponds to the signal output port.

In Fig. 13, we depict the response of the circuit from DC to 1 GHz with a solid line. The steep rise ensures the fundamental mode reflection at 56 MHz with effective damping of the first HOM at 168 MHz. The simulated transmission parameter of the 3D high pass filter model for all the cavity modes below 1 GHz is also shown on the same figure as solid squares. Initially, the simulation of the model and the lumped circuit match well, but differences develop for modes around 830 MHz. They are due to vacuum gaps in the assembly that add in extra capacitance components in the high frequency region. However, both results show more than a 70 dB reduction in the fundamental mode power and less than 10 dB reduction for all HOMs except the four modes around 830 MHz, for which the reduction is less than 25 dB. For RHIC operation, only one HOM coupler assembly has been fabricated and leak checked. This HOM coupler was installed on the cavity at the 8 o'clock location in Fig. 9.

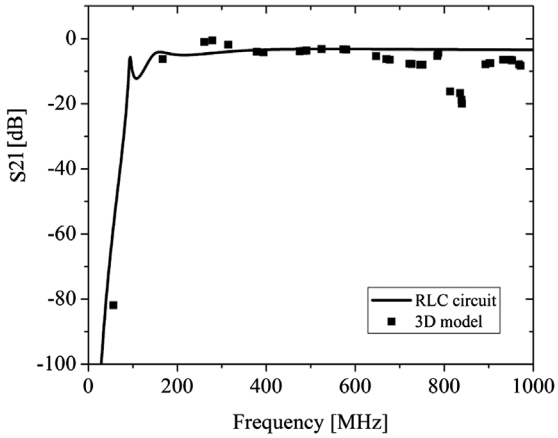


FIG. 13. S21 parameter of the 56 MHz cavity HOM high-pass filter.

## III. RHIC OPERATION

Due to limitations of the vertical test facility: the cryostat dimensions and available rf power, the cavity conditioning and rf measurements were completed after its installation into the cryomodule. Assuming that 19.5 W of rf power dissipation corresponds to 1 g/s increase in the helium flow rate, the quality factor $Q0$ of the cavity can be calculated at a measured voltage $V$ as

$$Q_0 = \frac{V^2}{19.5(F - F_0) \cdot R/Q} \tag{1}$$

where $R/Q$ is 80 Ohm, $F$ is the flow rate during operation measured in g/s in Eq. (1) at a voltage level $V$, and $F_0$ is the flow rate of the helium with the cavity at zero voltage, which is measured to be 1.95 g/s. The quality factor $Q_0$ of the cavity after rf conditioning is calculated to be $1 \times 10^8$. The cavity had multiple dedicated beam tests and was brought into RHIC operation after rf conditioning and further helium conditioning, which is discussed below.

### A. Operation without HOM coupler

At first, the cavity was tested with no HOM coupler installed. The cavity operated with 11 bunches of protons at a total intensity of $25 \times 10^9$ particles per bunch. The proton bunches were injected in an evenly distributed 12-bunch pattern, which provided maximum rf field damping between bunches. After extracting the fundamental mode damper, the cavity was slowly tuned toward the beam resonance from 40 kHz below the target frequency. The tuning ranges of the HOMs from the tuner are much larger than that of the fundamental mode. All monopole modes below 500 MHz, as listed in Table III, were excited across the full frequency sweep. Significant beam instability was observed from the effect of these HOMs as they are excited over the tuning process.

TABLE III. Excited monopoles measured during cavity tuning toward beam resonance.

| Frequency (MHz) | $R/Q$ (Ω) | Full tuning range (kHz) | Cavity fund. freq. across tuning range with HOM excited (MHz) |
|---|---|---|---|
| 165.9 | 34 | 848 | 56.2647, 56.2929, 56.2935, 56.2959 |
| 274.0 | 29 | 299 | 56.2671, 56.2696, 56.2760 |
| 377.1 | 30 | 447 | 56.2799 |
| 474.8 | 25 | 420 | 56.2962 |

The cavity frequency was tuned and parked at less than 1 kHz away from the beam resonance line. The final bunch length of the proton beam increased by 2.7 times of the original size, and significant beam loss occurred at each HOM excited frequency, as shown in Fig. 14. The beam profile change was recorded by the wall current monitor, which measures the broadband resistive signals as the bunches pass by. The signals are sampled and digitized to reconstruct the longitudinal profile of the bunches. A comparison of beam profiles before and after multiple HOMs were excited through the tuning process is shown in Fig. 15.

No dipole or higher order modes were observed during the cavity operation, and the HOM power beyond 500 MHz was considered negligible. The rf amplifier was turned off during the cavity operation.

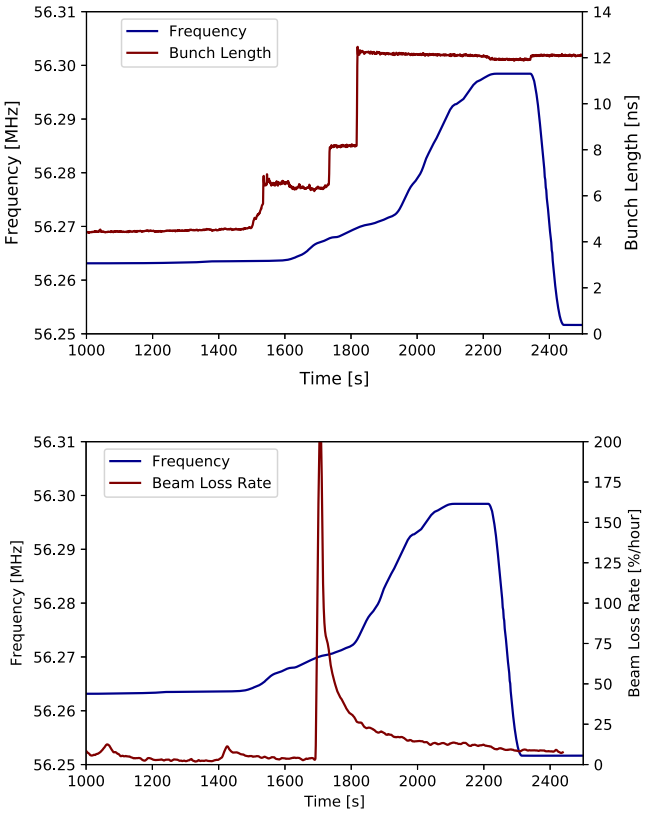


FIG. 14. Both the bunch length (top) and beam loss rate (bottom) increase as cavity frequency swept through full tuning range.

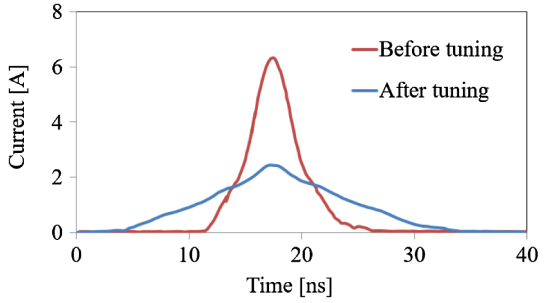


FIG. 15. Beam profile decay from 40 kHz cavity detuning toward the beam resonance line.

### B. Operation with HOM coupler

The cavity was commissioned with one HOM coupler installed. Viewing from the coupler port side, the HOM coupler is 45 degrees clockwise from the fundamental mode damper. The cavity gap voltage was limited to 300 kV, due to the HOM coupler thermal quench, compared with the planned operational voltage of 2 MV. Table IV lists the typical beam parameters.

A signal from the HOM coupler was measured during operation of the cavity, with full RHIC beam and cavity voltage set at 300 kV. From the results shown in Table V, the rf performance was very close to the design after fabrication, tuning, and cool down to 4 K. The discrepancy between simulations and measurements is due to many factors, including difference in frequency, beam intensity, and spectrum distribution. Over the entire frequency tuning to the beam resonance, the cavity has successfully maintained the beam intensity and shape with this single coupler providing sufficient damping to all dangerous HOMs.

TABLE IV. RHIC operation parameters.

| | Au + Au | $^3$He + Au | |
|---|---|---|---|
| | Au (b/y) | He in blue ring | Au in yellow ring |
| Intensity ($\times 10^9$) | 180 | 450 | 180 |
| Energy (GeV) | 100 | 103 | 100 |
| Bunch length w/o 56 MHz cavity (ns) | 4.5 | 6.0 | 4.5 |
| Bunch number | 111 | 111 | 111 |

TABLE V. Power comparison for each mode from the HOM coupler output during operation.

| Mode # | Frequency (MHz) | $Q_{\text{ext simulation}}$ | $Q_{\text{ext measured}}$ | $P_{\text{simulation}}$ (W) | $P_{\text{measured}}$ (W) |
|---|---|---|---|---|---|
| 1 | 56.31 | $4.1 \times 10^{10}$ | $3.5 \times 10^{10}$ | 1.0 | 2.52 |
| 2 | 166.23 | 2031 | 6896 | 3.59 | 4.06 |
| 3 | 273.77 | 2593 | 6313 | 0.023 | 0.033 |
| 4 | 376.76 | 3359 | 17 349 | 0.0016 | 0.000 87 |
| 5 | 474.20 | 4142 | 2132 | 0.0063 | 0.000 96 |
| 6 | 573.54 | 6895 | 11 490 | 0.000 20 | 0.000 089 |
| 7 | 678.94 | 4850 | 13 497 | 0.000 063 | $<1 \times 10^{-5}$ |

Even with the six-fold lower cavity voltage during the Au + Au run, a reduction in bunch length and an increase in luminosity, reflected by the zero degree calorimeter (ZDC) rate of the detectors, are observed clearly as the cavity is turned on, as illustrated in Fig. 16. The bunch length of both beams shrank by about 4.5%, when the 56 MHz cavity was turned on. The hourglass effect, which refers to the increase of the betatron function and the size of the transverse beam away from the IP therefore, is reduced. Consequently, the luminosity is enhanced by about 3%, as measured by the ZDC coincidence rate. A similar observation was made in the $^3$He + Au run.

Beam simulations were performed for the 56 MHz cavity voltages of 300 kV and 2 MV. The simulated luminosity and bunch pattern are shown in Fig. 17. Effects included in simulations are intrabeam scattering, cavity wakefields, and stochastic cooling. Parameters used in these simulations reflect those during the normal operation of RHIC.

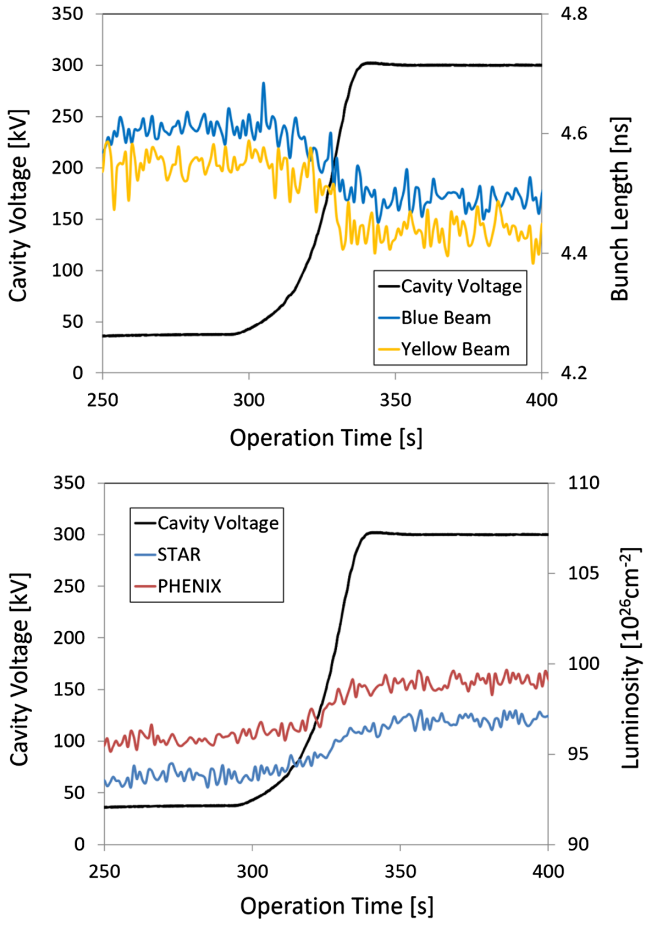


FIG. 16. Reduction of the bunch length of both beams in RHIC (top) and the resulting improvement in luminosity (botttom) observed by two detectors (STAR and PHENIX) as the 56 MHz cavity voltage was slowly ramped up.

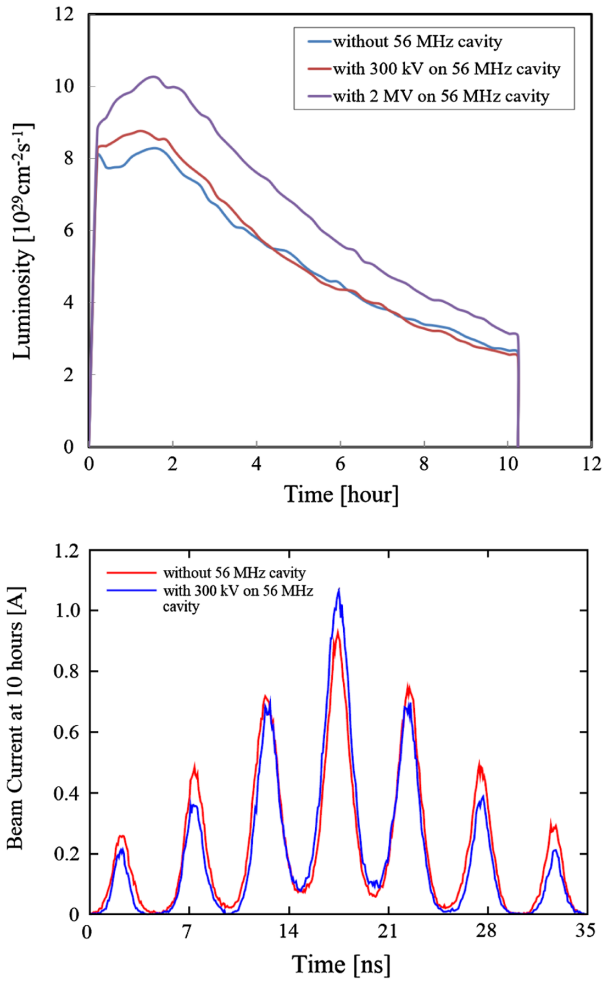


FIG. 17. Simulations of the RHIC luminosity (top) and bunch pattern (bottom) at different voltages of the 56 MHz cavity.

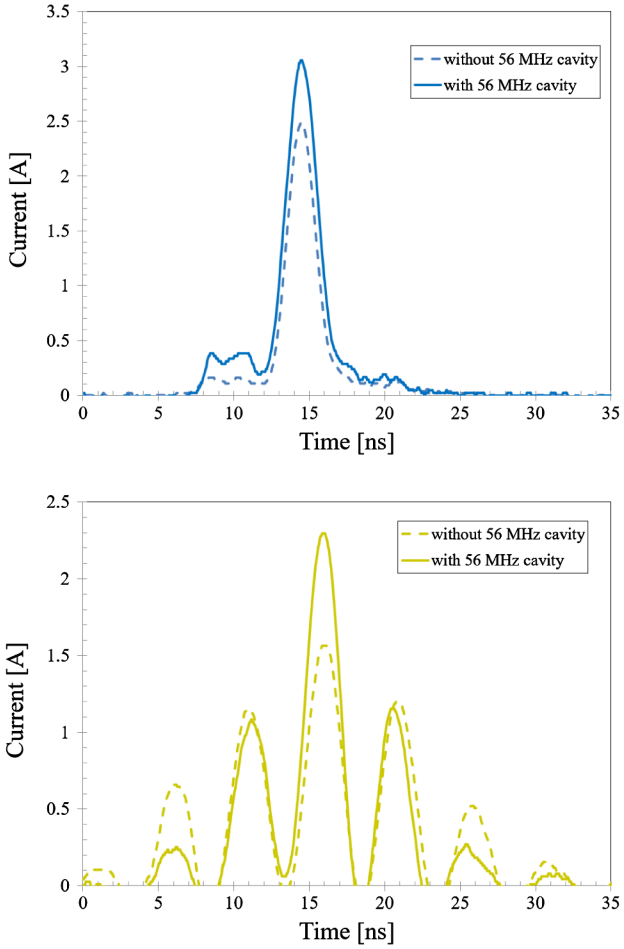


FIG. 18. The longitudinal profile of the $^3$He beam (in blue ring, top) and the Au beam (in yellow ring, bottom). The solid lines and dashed lines correspond to operation with the 56 MHz cavity on and off, respectively.

The results indicate a 5% luminosity increase when the 300 kV is applied to the beam. This agrees well with our experimental observations. The same simulation tool also predicts that the luminosity will be 30% higher if the full 2 MV gap voltage is reached.

The simulations also predict change of the population of ions in different 197 MHz rf buckets when the Au beam is rebucketed. Population of the particles in the satellite buckets is reduced because the bunch length is squeezed by the 56 MHz cavity. We also observed this population difference, between turning on/off the 56 MHz cavity at the end of the store time (about ten hours), using a wall current monitor, as shown in the bottom of Fig. 18. The decrease in the bunch length is 4%.

With the full current beam in RHIC, a total power extracted from the single HOM coupler was measured as 4.1 W. An extracted power at the fundamental frequency was 2.5 W, corresponding to an external $Q$ of $4 \times 10^{10}$. All HOMs under 600 MHz with a power of 0.8 mW or higher were identified using a spectrum analyzer; the HOMs at higher frequencies were below the measurement resolution. No measurable degradation of the RHIC beam due to the HOMs from the 56 MHz cavity was observed.

The cavity operation with HOM coupler was limited by a thermal quench at 330 kV. The early quench indicates that conduction cooling of the coupler is insufficient. Thermal analysis of the temperature signal from the sensor located on the HOM coupler flange indicated that the local heating may come from the braze material on the sapphire vacuum seal window. The sapphire window was then removed from the HOM coupler assembly, and the filter section had new vacuum sealing arrangement to accommodate the extension of the cavity vacuum through the entire filter. However, a cold test of the cavity with the modified HOM coupler had only reached 430 kV before a thermal quench. The heat source was suspected to be the contamination on the surfaces exposed to high magnetic field region, which needs further investigation and well planning of chemical treatment.

### C. Using FMD for HOM damping

While the source of the HOM coupler heating is under investigation and the coupler redesign is in progress, it was decided to experiment with using FMD for HOM damping during the cavity operation in 2016. As FMD couples strongly not only to the fundamental, but also to higher order modes, it can be used for HOM damping during system turn-on. The goal was to demonstrate 1 MV gap voltage. This operation required a detailed mapping of the high order mode landscape, full understanding of the dynamic system stresses during system turn-on, optimization of the FPC coupling to provide enough active frequency stabilization while minimizing extracted power. The maximum voltage reached with this method was 1 MV, limited by the rf power extraction via the FMD cable. A significant improvement of longitudinal focusing was demonstrated as indicated in Fig. 19 by reduced particle population in satellite buckets of the 197 MHz system [16].

### D. Helium processing

Helium processing is a well-developed technique for performance improvement of SRF cavities [17], which was

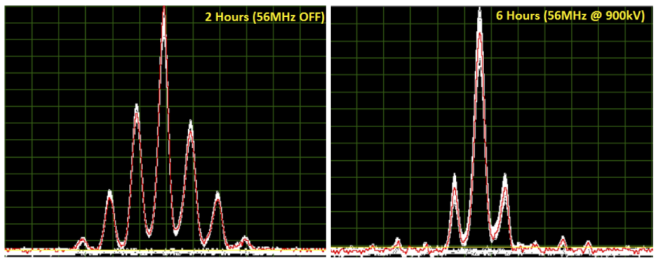


FIG. 19. The longitudinal profile of the RHIC beam with the 56 MHz system off (left) and on with FMD engaged for HOM damping (right).

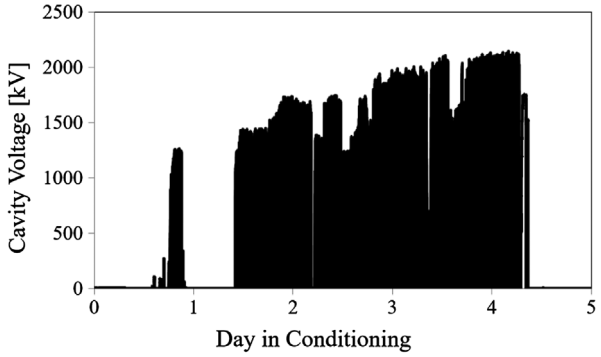


FIG. 20. Helium conditioning progress in 56 MHz cavity under pulsed and CW modes.

successfully used at various facilities [18–20]. The large inner volume of the 56 MHz cavity makes it difficult to establish a high-quality, field-emissionfree rf surface after buffered chemical polishing and high pressure rinsing. Along with high power conditioning, *in situ* helium processing is often used to achieve higher rf gradient. We established a helium partial pressure of $1 \times 10^{-5}$ torr in the cavity, while baseline pressure was measured below $2 \times 10^{-10}$ torr at 4 K. Helium gas was introduced into the cavity via a turbo pumping port, and the gas inlet valve was precisely controlled and monitored. The cavity operated with gradually increasing rf power during the addition of the helium gas for 74.5 hours accumulated. The conditioning alternated between pulsed and continuous wave rf input signals.

During the entire conditioning process, helium flow is controlled below 10 g/s to limit the heat load under an acceptable level by the cryogenic system. The peak cavity gradient level with low field emission improved by 33% from the helium-ion surface cleaning affect alone, as shown in Fig. 20. This increase of the voltage in the cavity corresponds to the improvement of the cavity quality factor under the same helium consumption. With the dynamic cryogenic heat loss set to 40 W at 4.5 K, the conditioning with rf power only for an accumulated 31 hours, the cavity reached 0.97 MV in CW mode and a corresponding $Q_0$ around $1.2 \times 10^8$. After the helium conditioning, the maximum voltage increased to 1.93 MV and the $Q_0$ to $3.0 \times 10^8$.

Thus, the helium processing allowed the cavity to reach its design voltage. During beam operations, the accelerating voltage was limited not by the cavity performance, but by the HOM coupler thermal quench.

## IV. SUMMARY

We successfully designed, installed, and commissioned the first QWR SRF cavity in RHIC. This was also the first application of a superconducting QWR in any storage ring. The design of the cavity began in 2009 as the first Accelerator Upgrade Project for RHIC in SRF science and technology. The cavity was installed in the collider and commissioned eight years later with most of its design features working well. The only item which failed to achieve the design specifications was the HOM damper due to a thermal issue that prevented high field operation. Nevertheless, the HOM damper still fulfilled all the rf expectations by sufficiently damping all HOMs through the cavity tuning range.

The 56 MHz cavity is one of the lowest frequency QWRs in operation. With large surfaces and coaxial-like geometry, the design has innovative corrugations on the cavity that suppress multipacting zones in the main cavity volume. The cavity geometry and dimension also put a challenge on the mechanical structure design to reach an extremely low Lorentz coefficient of $-33$ Hz/MV$^2$ and pressure detuning coefficient of $-0.282$ Hz/mbar [21,22]. Precise and relative large tuning of such low frequency cavity under cryogenic temperature is achieved by employing a thin, easily deformable tuning plate that is not subjected to differential pressure forces, and by a combination of stepper-motor and piezo-electric actuators. Extensive and careful analysis was carried out to ensure the mechanical lifetime of this mechanism.

As the cavity resonance crosses several beam spectrum lines during energy ramping, a unique fundamental mode damper is was designed to suppress the fundamental mode impedance. The HOM damper is also a novel design implementing sapphire ring capacitors to minimize the 3-stage Chebyshev high-pass filter to a workable dimension. The robust design of HOM coupler is insensitive to the manufacturing errors and frequency changes during fabrication and chemical processing, as was verified by the rf measurements after installation. The initial beam tests showed a luminosity increasing of 3%, and a bunch length shrinking of 4% at 1/6 of the design cavity voltage. The HOMs were very efficiently damped under full beam current.

However, the cavity operation with the HOM coupler was limited by the HOM coupler thermal quench at 330 kV. Removing the sapphire window with normal conducting brazing material improved the quench limit to only 430 kV. Further investigation of the coupler heating issue and coupler redesign are in progress. Meanwhile an experiment was performed with using FMD for HOM damping. The experiment was successful demonstrating sufficient suppression of higher-order-mode impedance, achieving the gap voltage of 1 MV, and reducing particle population in satellite buckets of the 197 MHz system [16]. The 56 MHz system upgrade with redesigned HOM damping and improvements in other subsystems is planned to be complete and ready for beam operation at full accelerating voltage by late 2021.

## ACKNOWLEDGMENTS

This works is supported by Brookhaven Science Associates, LLC under Contract No. DE-AC02-98CH10886 with the U.S. DOE. The authors would like

to acknowledge all the support from cavity fabrication, post processing, and most of all, the RHIC control room support on the cavity operation. The authors would like to thank Gary McIntyre, Scott Seberg, Richard Tallman, and Harold Dorr on the processing, assembly, and installation of the 56 MHz cavity cryomodule. The authors would also like to thank Naeem Huque, Edward Daly, and Haipeng Wang at Jefferson Lab for their full support in HOM coupler fabrication and room temperature measurements.

[1] *Relativisitic Heavy Ion Collider Configuration Manual*, Brookhaven National Laboratory, Final ed. (2006).
[2] I. Ben-Zvi, *Proposal: 56 MHz RHIC SRF cavity*, Technical Report (Collider Accelerator Department, Brookhaven National Laboratory, 2007).
[3] A. Fedotov and I. Ben-Zvi, in *Proceedings of the 23rd Particle Accelerator Conference, Vancouver, Canada, 2009* (IEEE, Piscataway, NJ, 2009), pp. 2483–2485.
[4] K. W. Robinson, Instability of beam in radiofrequency systems, Cambridge Electron Accelerator Technical Report No. CEAL-1010, 1964.
[5] S. R. Koscielniak, Part. Accel. **62**, 179 (1999).
[6] M. M. Karliner, V. E. Shapiro, and I. A. Shekhtman, Sov. Phys. Tech. Phys. **11**, 1501 (1967).
[7] V. E. Shapiro, Sov. Phys. JETP **28**, 301 (1969).
[8] N. Towne, Longitudinal stability with, and higher-order mode damping of, superconducting storage cavities in RHIC, Collider Accelerator Department, Brookhaven National Laboratory Technical Report, 2008.
[9] I. Ben-Zvi, Superconducting storage cavity for RHIC, Collider Accelerator Department, Brookhaven National Laboratory Technical Report No. C-A/AP/337, 2009.
[10] X. Chang and I. Ben-Zvi, Geometric optimization of the 56 MHz SRF cavity and its frequency table, Collider Accelerator Department, Brookhaven National Laboratory Technical Report No. C-A/AP/331, 2009.
[11] D. Naik and I. Ben-Zvi, Suppressing multipacting in a 56 MHz quarter wave resonator, Phys. Rev. Accel. Beams **13**, 052001 (2010).
[12] Q. Wu, S. A. Belomestnykh, L. Ge, C. Ko, Z. Li, C. K. Ng, and L. Xiao, Conf. Proc. **C1205201**, 2477 (2012).
[13] Q. Wu, I. Ben-Zvi, C. Pai, and S. Bellavia, Conf. Proc. **C110328**, 916 (2011).
[14] Q. Wu and I. Ben-Zvi, Conf. Proc. **C100523**, 3081 (2010).
[15] Computer simulation technology, CST, Darmstadt, Germany, 2011.
[16] S. Polizzo, 56 MHz project overview and status update, Machine Advisory Committee Review (2016).
[17] H. A. Schwettman, J. P. Turneaure, and R. F. Waites, Evidence for surface-state-enhanced field emission in rf superconducting cavities, J. Appl. Phys. **45**, 914 (1974).
[18] D. W. Storm, J. M. Brennan, and I. Ben-Zvi, Superconducting resonators for the university of washington booster linac, IEEE Trans. Nucl. Sci. **32**, 3607 (1985).
[19] C. Reece, M. Drury, M. G. Rao, and V. Nguyen, Conf. Proc. **C970512**, 3105 (1997).
[20] O. Brunner, A. Butterworth, G. Cavallari, N. Hilleret, J. Jimenez, and J. Tuckmantel, in *Proceedings of the 8th Workshop on RF superconductivity, Abano Terme, Padua, Italy, October 6–10, 1997* (1998), pp. 133–137.
[21] C. Pai, Q. Wu, I. Ben-Zvi, A. Burrill, X. Chang, G. T. McIntyre, R. Than, and J. E. Tuozzolo, Conf. Proc. **C110328**, 907 (2011).
[22] C. Pai, 56 MHz SRF cavity and helium vessel design, 2nd External Review of 56 MHz SRF Storage Cavity (2011).